

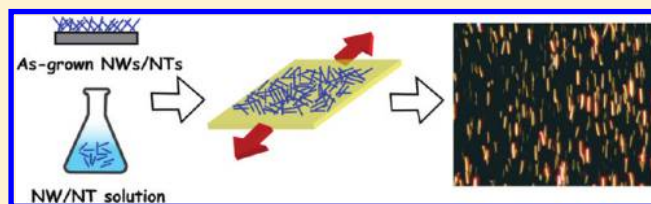
Stretched Contact Printing of One-Dimensional Nanostructures for Hybrid Inorganic–Organic Field Effect Transistors

Gen-Wen Hsieh,^{*,†,‡} JinJin Wang,[†] Ken Ogata,[†] John Robertson,[†] Stephan Hofmann,[†] and William I. Milne^{*,†}

[†]Engineering Department, University of Cambridge, 9 JJ Thomson Avenue, Cambridge CB3 0FA, U.K.

[‡]Institute of Lighting and Energy Photonics, National Chiao Tung University, No. 301, Gaofa third Rd., Guiren Township, Tainan County 71150, Taiwan, R.O.C

ABSTRACT: We demonstrate a stretched contact printing technique to assemble one-dimensional nanostructures with controlled density and orientation from either dry or wet sources. The random, chaotically arranged nanostructures can gradually transform to a highly aligned configuration. Our results show that up to 90% of the printed nanowires are aligned within $\pm 15^\circ$ of the primary stretching direction. This approach is easily applicable to a variety of nanowires and nanotubes on different substrates, and we demonstrate various field effect transistors with nanowire and hybrid nanowire–polymer networks. The hybrid inorganic–organic transistors based on a parallel aligned nanowire network and a semiconducting polymer revealed a significant enhancement in transistor mobility, a 10-fold reduction in subthreshold slope (~ 0.26 V decade⁻¹), and superior air stability compared to a pristine polymer host.



INTRODUCTION

The drive toward “ubiquitous electronics” that has been motivated by the rise of mobile communications and enabled by high quality displays has led to a commercial need for a new large area, flexible, cost-effective, and sustainable electronic technology. Several new materials systems are competing such as large grained silicon films, metal oxides, one-dimensional (1-D) nanostructures, and organic semiconductors. Organic semiconductors have, notably, been promoted as the potentially superior technology as they are compatible with very low cost patterning technologies based on printing.^{1,2} However, they suffer from low mobility and poor air stability compared with inorganic alternatives.^{3–5} Hence, a number of groups are investigating the use of nanostructured composite materials in which an inorganic nanomaterial is incorporated with an organic semiconductor with the aim of retaining the patterning advantages of the organic host, while enhancing performance by a path through the inorganic material.^{6–12}

To enable the advancement of these hybrid material systems, one of the most important challenges is to manipulate nanoscale structures into a parallel aligned network which, in the active channel of transistors, could help charge transport without disturbing the orientation of organic conjugated molecules/polymers. Recent reports on nanostructure alignment have showed a broad range of proof-of-concept self-assembly approaches. Wet solution-based assembly methods via microfluidic alignment,^{13–16} electric/magnetic field directing,^{17–22} Langmuir–Blodgett films,^{23–25} blown bubble films,^{26,27} and anisotropic evaporation of cylindrical droplets²⁸ have been studied. However, achieving spatially specific, highly ordered 1-D nanostructure arrays from solution still continues

to be a significant challenge. Relatively simple dry assembly methods by shear-sliding contact printing^{29–32} and roll printing^{33–35} were recently developed to directly transfer regular arrays of 1-D nanomaterials from donor (mainly for vertical aligned networks) to receiver substrates. A polydimethylsiloxane (PDMS)-mediated or adhesive tape-assisted soft contact printing^{36–41} was also conducted, which demonstrated the large area capability of transferring prealigned (formed by guided growth during nanostructure synthesis) horizontal arrays. While these approaches are successful for assembling single layer arrays of functional NW/NT devices, the development of a comprehensive assembly approach dealing with both wet-based and dry-based 1-D nanomaterials remains a challenge.

Here we demonstrate a stretched contact printing technique to assemble 1-D nanostructures with controlled orientation and density from either as-grown substrates or solution-based dispersions. Unlike recent work on strain-release assembly of nanowires which relied on repeated operation of material transfer to prestrained substrates and strain release,⁴² our process is based on a simple one-step stretching of an elastic substrate covered with high-aspect ratio nanostructures. During the stretching process, the randomly orientated nanostructures gradually transform to highly aligned films. Subsequently, these stretching-aligned 1-D nanostructures can be transferred to other rigid or flexible substrates, forming a single layer of well-oriented network. Our results show that up to 90% of the

Received: October 27, 2011

Revised: February 18, 2012

Published: February 21, 2012

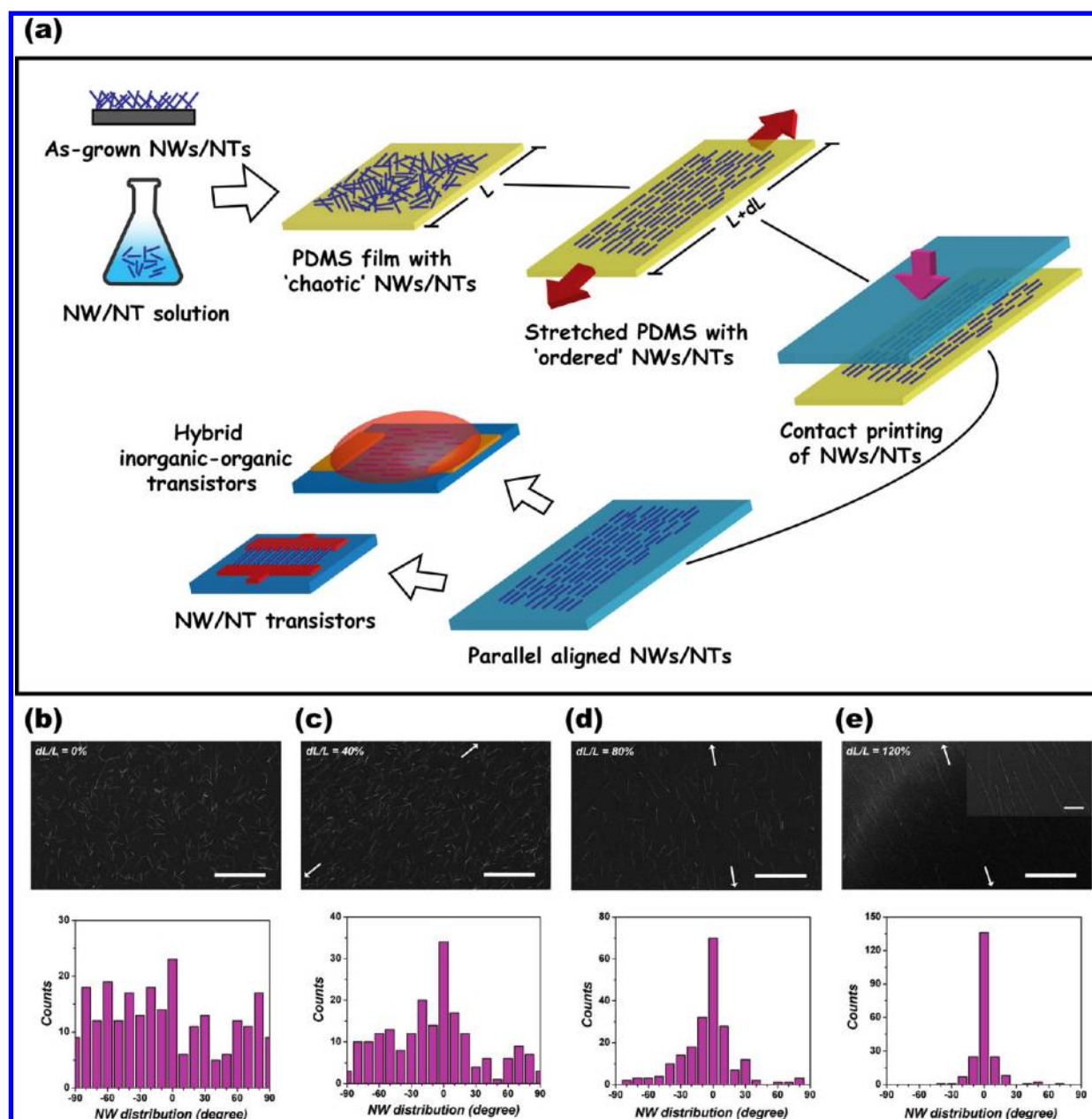


Figure 1. Stretched contact printing. (a) Schematic illustration of process flow for the stretched contact printing of as-grown or solution-based 1-D nanostructures. (b–e) Resulting SEM images and the corresponding alignment histograms of the ZnO NWs transferred from different stretching conditions (%): (a) S0: 0%; (b) S1: 40%; (c) S2: 80%; and (d) S3: 120%, where each arrow pair indicates the stretching direction. Scale bar: 10 and 2 μm (inset).

printed NWs are aligned within $\pm 15^\circ$ of the primary stretching direction. Moreover, the feasibility of incorporating these stretching-aligned networks with organic semiconductors for generating field effect transistors (FET) devices is demonstrated. Through addition of such ordered networks to organic semiconductors, the flow of electric current can be accelerated, resulting in an enhancement of transistor mobility and of device stability in ambient air conditions.

EXPERIMENTAL METHODS

Preparation of As-Grown Nanowires. The n-type zinc oxide (ZnO) NWs with diameters of ~ 50 – 80 nm were prepared by vapor phase deposition. ZnO powder mixed with graphite at a ratio of 1:1 was placed at the center of a quartz reaction tube heated to 950°C in a flow of Ar/O₂ (50/1 sccm)

at a total pressure of 3 mbar. NW growth was promoted downstream on a Si substrate covered by a 1 nm thick gold layer.¹⁰

Intrinsic Si NWs with diameters of ~ 10 – 60 nm and ~ 5 μm in length were synthesized by chemical vapor deposition using hydrogen diluted silane (H₂/SiH₄ ratio of 170/30 sccm, total pressure 15 mbar) at 400°C and a 2 nm thick gold layer as catalyst on a thermally oxidized Si (200 nm SiO₂) wafer support.⁴³

A PDMS film (~ 2 – 4 mm thick) was formed by casting its prepolymer (Sylgard 184, Dow Corning), mixed with curing agent at a ratio of 15:1 (w/w), degassing in a vacuum oven for 30 min over a plastic mold, and curing in the oven at 50°C for 4–6 h. The PDMS film was placed on top of the NW growth substrate, and after applying gentle manual pressure from the

top, the film was quickly peeled to transfer the NWs to the PDMS surface (yield: 50–60%).

Dispersions of Nanowires and Nanotubes. The *N,N*-dinitridicperylene-3,4,9,10-tetracarboxylic diimide (PTCDI-C13, Aldrich) NWs were prepared by adding methanol to a vial containing the solutions of PTCDI in chloroform (1.5 mg mL⁻¹) to induce the precipitation and self-assembly by π - π interactions of PTCDI.⁴⁴ The bottom layer of the vial contains PTCDI dissolved in chloroform, and the upper layer contains methanol. An initial swirl of the vial immediately induced the supramolecular self-assembly into 1-D nanostructures, and in several minutes, the complete formation of NWs was observed. The beltlike PTCDI NWs were typically 50–110 nm in width and tenths of micrometers in length.

Single-walled carbon nanotubes (CNTs) (CoMoCAT, South Nanotechnologies) were suspended in aqueous sodium dodecyl benzene sulfonate (SDBS; 1 wt %) where the concentration was typically 10 mg mL⁻¹ with an average bundle length of 1.0–2.0 μ m and a diameter of \sim 10 nm. No further purification steps were carried out after the suspension. These nanostructures were transferred to the PDMS films by drop-casting and dried at room temperature overnight.

Stretched Contact Printing for Assembling Nanowires and Nanotubes. The controlled stretched contact printing was carried out using a home-built setup consisting of two foldback clips, each fixed with a movable carrier that can easily be shifted along the length of a scale-engraved rail. The PDMS films with a random distribution of NWs (by stamping or casting) were held with two foldback clips and stretched to different distances at a controlled speed. NWs were transferred to the surface of a rigid Si/SiO₂ substrate (functionalized by poly(L-lysine) to increase the yield³⁰) or a flexible sheet by stamping and then peeling back the PDMS at a relatively slow speed, forming a single layer of oriented NWs on the receiving substrate.

Nanowire and Nanocomposite Transistors. For nanowire transistors, ZnO NWs and Si NWs were transferred to Si substrates covered by 120 nm thick SiO₂ ($C_i = 23$ nF cm⁻²). Source and drain contacts were defined by e-beam lithography and thermal evaporation (50 nm thick Cr for ZnO NW, 50 nm thick Ni for Si NW). The Si NW samples were dipped in a HF solution for 10 s to remove the native oxide prior to the metallization. Reliable contact formation was promoted by subsequent annealing in an Ar atmosphere at 425 °C for a few minutes, leading to a Ni silicidation of the Si NWs.⁴⁵

For hybrid inorganic–organic nanocomposite transistors, the Cr/Au contacts were defined by conventional UV photolithography on Si/SiO₂ substrates with stretching-assembled Si NWs. Prior to the octyltrichlorosilane self-assembled monolayer (OTS-SAM) surface treatment the Si NW samples were dipped in a HF solution. An organic semiconductor poly(2,5-bis(3-alkylthiophen-2-yl)thieno[3,2-*b*]-thiophene) (PBTTT, Merck) was spin-coated (at 600 rpm for 5 s and then 1300 rpm for 50 s) in a 1,2-dichlorobenzene solution (7–8 mg mL⁻¹) onto substrates covered with the Si NWs and Cr/Au electrodes. The spin-coating was carried out inside a N₂ glovebox. Pristine PBTTT devices were also fabricated in the same manner without the stretched contact printing process. The devices were annealed at 180 °C in N₂ for 15 min.

Characterization of Nanowire and Nanocomposite Transistors. The NW/hybrid FET devices were electrically characterized under ambient air, in dim light at room temperature with a Cascade probe station equipped with an

Agilent B1500A analyzer. From the measured transfer characteristics (I_{DS} vs V_{GS}), the transconductance (g_m), threshold voltage (V_T), and effective field effect mobility (μ_{FE}) of the FETs were extracted using the following expressions governing the operation in the linear and saturation regions:

$$I_{DS,lin} = \mu_{FE} C_i \frac{W}{L} (V_{GS} - V_T) V_{DS}$$

$$g_m = \frac{\partial I_{DS,lin}}{\partial V_{GS}} = \mu_{FE} C_i \frac{W}{L} V_{DS} \quad (1)$$

$$I_{DS,sat} = \frac{1}{2} \mu_{FE} C_i \frac{W}{L} (V_{GS} - V_T)^2$$

$$g_m = \frac{\partial I_{DS,sat}}{\partial V_{GS}} = \mu_{FE} C_i \frac{W}{L} (V_{GS} - V_T) \quad (2)$$

where I_{DS} is the drain current, V_{GS} the gate-source voltage, V_{DS} the drain-source voltage, C_i the gate dielectric capacitance per unit area, W the channel width, and L the channel length. The hybrid NW–polymer and pristine polymer FETs were further characterized by tapping mode atomic force microscopy (Explorer, Veeco).

RESULTS AND DISCUSSION

Stretched Contact Printing. Figure 1 shows the processing steps for creating oriented NW/NT arrays from a wafer source or solution and transferring them to another rigid or flexible substrate. The sources of nanostructures were either as-grown randomly oriented forests (e.g., ZnO NWs, Si NWs) or solution-based dispersions (e.g., CNTs, organic NWs). The first step comprised the stamping of as-grown NWs, or casting of nanostructure dispersions, onto PDMS films, which generated a layer of randomly distributed NWs or NTs. The PDMS film, with initial length (L), was then held with two foldback clips and gently stretched to different lengths. During this process, the randomly orientated nanostructures were gradually transformed to a partially ordered and further to a highly aligned film, according to the extent of deformation of the elongated PDMS film (defined as $L + dL$, where dL is the increase in length of the PDMS film due to stretching). These NWs/NTs were then transferred to the surface of a rigid Si substrate or a flexible film by stamping, providing a single layer of oriented nanostructures. The difference between the PDMS–nanostructure and substrate–nanostructure van der Waals interactions enables an efficient transfer process.³⁶ Thus, the extent of stretching that can induce the alignment effect simply depends on the length and density of the employed nanostructures and the elasticity of the PDMS stamp.

Figures 1b–e show SEM images of ZnO NW arrays transferred on Si/SiO₂ substrates for increasing dL/L ratios. The histograms present the average alignment success for over 200 NWs, as determined from an area of 10 μ m \times 10 μ m for at least five arbitrary locations over the entire printed area (\sim 10 mm \times 10 mm) on the receiver substrates. The networks printed from a less stretched PDMS film ($dL/L = 40$ –80%) display modest alignment effects of ordering 25–48% of the NWs within $\pm 10^\circ$ from the elongated axis of the elastic film (Figure 1c,d), while those from a nonstretched film ($dL/L = 0\%$) show a random distribution (Figure 1b). For the networks transferred from the more highly stretched ($dL/L = 120\%$) PDMS film, as shown in Figure 1e, the angle distribution

histogram shows that more than 78% of the NWs are aligned within $\pm 10^\circ$ of the primary stretching direction, and over 90% of NWs are within $\pm 15^\circ$. Table 1 summarizes the average

Table 1. Average Alignment Results Based on Different Stretching Conditions

sample type	stretch extent (dL/L, %)	NW coverage (per $10 \times 10 \mu\text{m}^2$)	avg. NW alignment (%), within		
			$\pm 5^\circ$	$\pm 10^\circ$	$\pm 15^\circ$
S0	0	50	10	13	18
S1	40	42	17	25	32
S2	80	26	33	48	62
S3	120	21	65	78	90

alignment results based on the different stretching conditions. Note that the NW areal density decreases from 50 NWs to 20 NWs per $10 \mu\text{m} \times 10 \mu\text{m}$ depending upon the elongation. Hence, the orientation and density of the NWs in the stretched film will mainly follow the elongating direction.

Moreover, the separation between the parallel aligned NWs can further be controlled by a secondary contact printing stretched in an orthogonal direction. As shown in Figure 2,

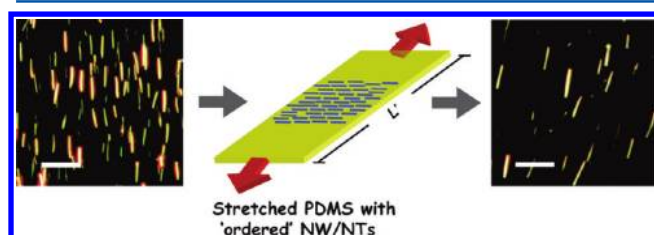


Figure 2. Secondary contact printing stretched in an orthogonal direction for separation control. Left: NW arrays before stretching; Right: NW arrays after stretching. Scale bar: $10 \mu\text{m}$.

another elastic PDMS film was applied onto a substrate with a single layer of highly oriented NWs, whereby the alignment direction of the NWs is perpendicular to the initial elongating direction of the PDMS. The action of this secondary printing will be to simply expand the separation space of these aligned NWs. For example, an initial NW network separation of $\sim 2\text{--}3 \mu\text{m}$ was increased to $\sim 4\text{--}6 \mu\text{m}$ by the stretching process ($dL'/L' = \sim 100\%$, where, similarly, dL' stands for the increased length of the PDMS film in the orthogonal direction). This separation-controllable feature can be applied to the fabrication of large area regular nanodevice arrays to make a much more efficient use of the 1-D nanostructures. However, it should be noted that nonfully aligned NWs might become more disordered due to this orthogonal elongation procedure.

Other 1-D Nanostructures by Stretched Contact Printing. To highlight the generality of our approach, we transferred a variety of 1-D nanostructures from either as-grown substrates or solution dispersions. Figure 3a shows that high density, ordered, uniform single layered Si NW networks were achieved by using the stretched contact printing method on as-grown randomly oriented Si NWs. Figure 3b,c shows good alignment also for solution-based single-walled CNTs and organic conjugated PTCDI NWs, both of which were drop-cast on PDMS films prior to the stretched contact printing process. Other work using dispersed and solution-synthesized NWs is in progress. We highlight that our approach is also applicable to

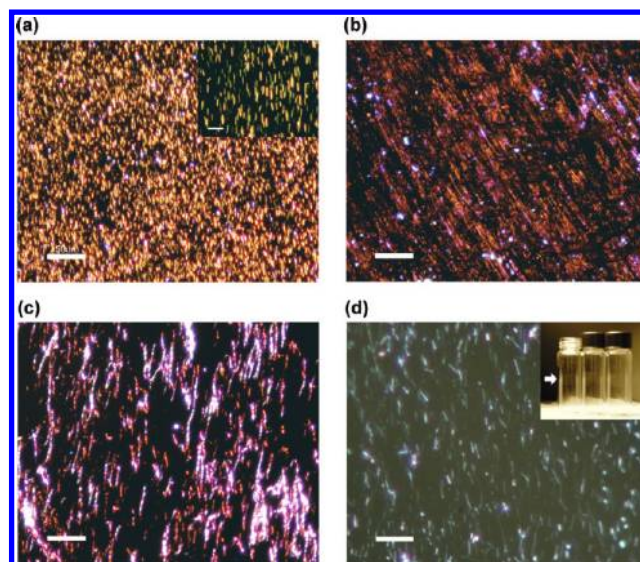


Figure 3. Dark field optical images of different aligned 1-D nanostructures by stretched contact printing. (a) Si NW arrays transferred from an as-grown substrate. Scale bar: 50 and $10 \mu\text{m}$ (inset). (b) Single-walled CNT arrays transferred from a randomly dispersed solution. Scale bar: $50 \mu\text{m}$. (c) Organic PTCDI NW arrays transferred from a randomly dispersed solution. Scale bar: $50 \mu\text{m}$. (d) Optical images of parallel aligned ZnO NWs on the surfaces of three glass cylinders. Scale bar: $10 \mu\text{m}$.

form various types of multilayer arrangements (e.g., crossbar, triangle) of 1-D nanostructures (data not shown here).

Taking advantage of the conformal contact offered by the soft PDMS films, we also used the stretched contact printing approach to transfer aligned NW or NT films onto both nonplanar and flexible substrates. In Figure 3d, for example, a single layer of ZnO NWs was transferred to the surface of a glass vial (by rolling a vial on a stretched PDMS film including assembled NWs). The as-transferred NWs are highly aligned and have uniform separation across the entire substrate.

The data clearly show that our stretched contact printing approach has several important advantages, including low-temperature processing and applicability to a wide range of substrates and 1-D nanomaterials. Importantly, for the latter our approach is applicable both to solution-based dispersions and as-grown samples supported on substrates.

Nanowire Transistor Arrays. In order to demonstrate the potential application of this stretched contact printing approach for electronic devices, we fabricated single- and multi-NW FET arrays based on the highly aligned NWs. We characterized FETs based on individual ZnO NWs (Figure 4a), which show typical n-channel transistor behavior. Figure 4b shows transfer and output characteristics for a typical FET based on $\sim 5\text{--}7$ aligned Si NWs. The device exhibits ambipolar behavior, with comparable ON currents for holes and electrons, showing that the accumulation of both holes and electrons occurs for negative and positive gate voltages, respectively. The hysteresis effect for those NWs is well-known^{14,46,47} and is thought to be due to charge traps at the surface of the nanostructures, especially when the measurement is carried out in air without passivation. Nevertheless, these results illustrate the viability of making nanodevices via the stretched contact printing technique. More work on large area NW transistor arrays and their application on logic devices will be reported at a later date.

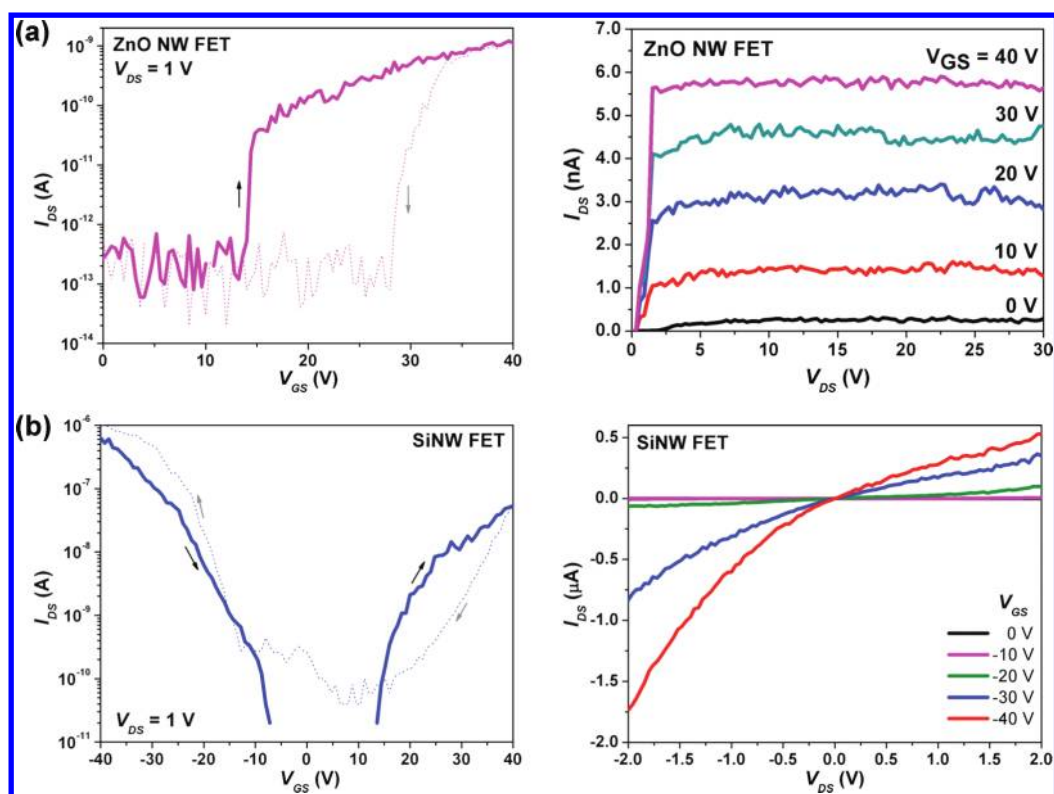


Figure 4. Transfer and output characteristics of (a) a single-nanowire ZnO transistor with Cr contact and channel length of $2.0 \mu\text{m}$ and (b) a multinanowire Si transistor (5–7 NWs) with NiSi contacts with reduced channel length of $\sim 0.5\text{--}1.0 \mu\text{m}$.

Hybrid Inorganic–Organic Nanocomposite Thin Film Transistors. Stretching-aligned 1-D nanostructures can be used to produce hybrid inorganic–organic semiconducting composites with improved performance. Here we demonstrate hybrid inorganic–organic FETs with typical channel lengths (L) of $20 \mu\text{m}$ and widths (W) of $10\,000 \mu\text{m}$. The channel layer consisted of a stretching-aligned Si NW network (aligned parallel to the channel direction and with an average area density of ~ 20 NWs per $10 \times 10 \mu\text{m}^2$ with $\sim 1\text{--}1.5 \mu\text{m}$ separation) mixed with a solution-processable organic semiconductor PBTTT. The interdigitated (Cr/Au = $10 \text{ nm}/50 \text{ nm}$ thick) source and drain contact patterns were defined by photolithography and thermal evaporation onto Si/SiO₂ substrates covered with transferred Si NWs. Prior to deposition of PBTTT, the samples were dipped in HF and subsequently treated with OTS in a N₂ environment. After PBTTT spin-coating and device annealing (both carried out inside a N₂ glovebox), the electrical performance of these hybrid Si-PBTTT FETs was characterized in ambient air with dim light and compared to measurements on pristine organic PBTTT FETs. Note that no field effect was observed from these stretching-aligned NW networks, indicating that the source-drain electrodes were not directly connected by Si NWs.

Figure 5a,b shows the characteristics of the hybrid Si-PBTTT and PBTTT devices. The values of I_{DS} in the output characteristics of the Si-PBTTT FET are much higher than those of the pristine PBTTT device. The contact resistance effect observed at low V_{DS} is of similar order for both hybrid and organic devices and can be reduced by using surface modification for the electrodes.⁴⁸ The saturation field effect mobility of the pristine PBTTT extracted from the $I_{DS}\text{--}V_{GS}$ curves is $0.031 \text{ cm}^2 \text{ V}^{-1} \text{ s}^{-1}$, and the ON/OFF current ratio is 4×10^4 (note: the values are inferior to previously reported

results,⁴⁹ probably because the employed PBTTT material has been in the laboratory for more than three years). For the hybrid Si-PBTTT FET, its ON/OFF current ratio is 1×10^7 and the carrier mobility is increased to $0.101 \text{ cm}^2 \text{ V}^{-1} \text{ s}^{-1}$, representing a ~ 3 times enhancement over the pristine PBTTT device. Moreover, a much sharper subthreshold slope of $0.258 \text{ V decade}^{-1}$ is achieved for the hybrid device, which represents a 10-fold reduction with respect to that of the pristine device. This improvement in field effect mobility and subthreshold slope upon the addition of aligned Si NWs is probably due to the superior electrical properties of the NWs, where they serve to increase the overall speed of charge carrier transport in the active channel.

Tapping mode AFM images of the pristine PBTTT and hybrid Si-PBTTT films after annealing are shown in Figures 5c and 5d, respectively. The topography and the size and structure of the crystalline domains are similar for both films (see insets Figures 5c,d). The aligned Si NWs are clearly revealed in the phase image (Figure 5d). Our data indicates that stretching-aligned Si NWs are embedded in the polymer film without interrupting the formation of polycrystalline PBTTT domains. Hence, these Si NWs may serve as a speedy pathway to transport a certain amount of charge carriers in the active channel. We believe this to be the key mechanism contributing to the increase in field effect mobility with reduced subthreshold slope in the hybrid device.

The possible charge transport routes via the hybrid Si-PBTTT film are illustrated in Figure 6. The first route is via PBTTT polycrystalline grains (black path), and more significantly, the second route is via a combinational path of PBTTT-Si NW-PBTTT (red path), which is likely to be the most desired route to enhance the charge carrier transport. However, to gain access to the red path, it is very important to

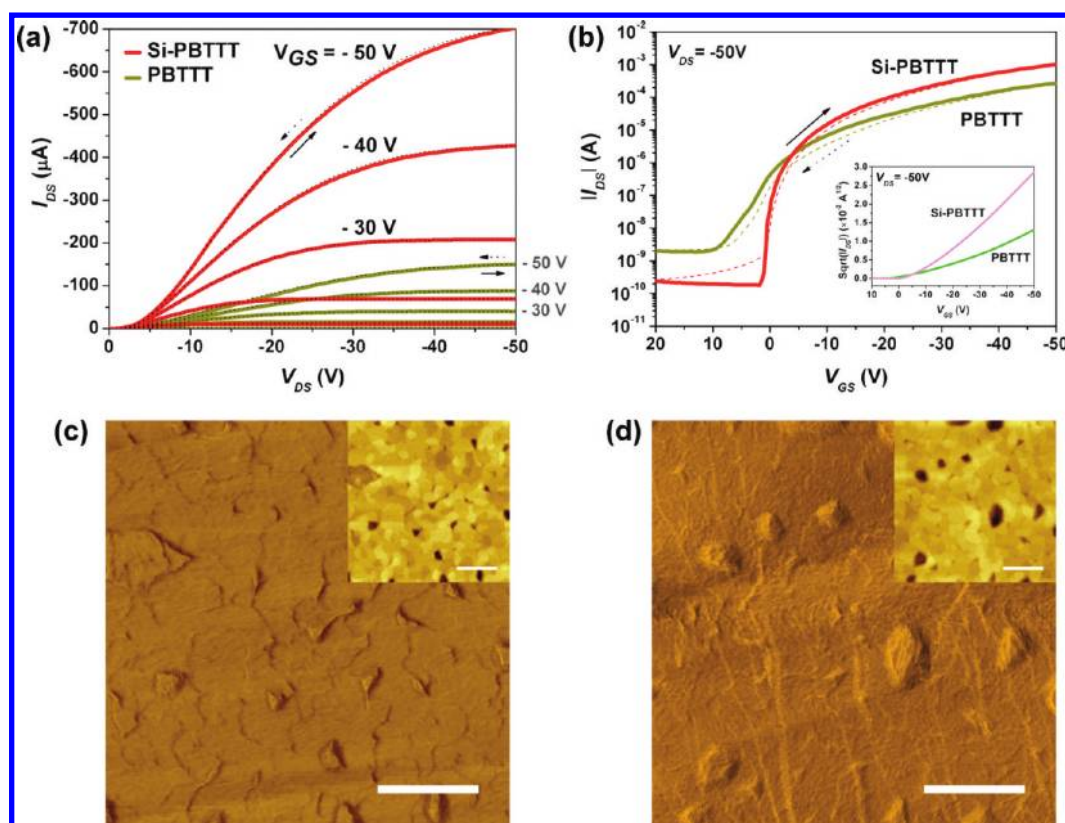


Figure 5. (a) Representative output characteristics of a hybrid Si-PBTTT FET and a pristine PBTTT organic FET. (b) Transfer characteristics of the same devices in the saturation regime at $V_{DS} = -50$ V. The measurement was performed at room temperature under ambient air environment, after N_2 annealing at 180°C for 15 min. The channel length and width of these devices are 20 and 10 000 μm , respectively. AFM phase images of (c) a PBTTT film and (d) a hybrid Si-PBTTT film after annealing (insets: topography). All images ($4 \mu\text{m} \times 4 \mu\text{m}$) are randomly acquired on the active channel area of the composite devices. Scale bar: 1.0 μm .

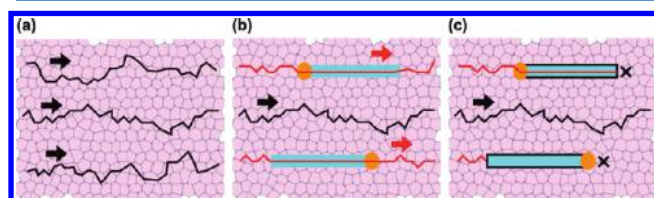


Figure 6. Schematic illustrations of possible charge transport routes via (a) crystalline PBTTT film (black-path), (b) crystalline PBTTT and semiconducting Si NWs (red path), where the NW oxide shell is removed by HF dipping, and (c) crystalline PBTTT and semiconducting Si NWs with oxide shell (red path prevented). Note: the orange dot is the Au catalyst used for NW growth.

remove the native silicon oxide shell surrounding each Si NW during the hybrid FET fabrication, as shown in Figure 6b. Otherwise, the oxide shell ($\sim 1\text{--}2$ nm thick) will inhibit charge transport (Figure 6c).

During the I - V measurements, we found that the output and transfer characteristics for hybrid Si (with oxide shell)-PBTTT

FETs were very similar to those of pristine PBTTT FETs, and no enhancement of, for instance, ON current, mobility, subthreshold slope was observed. Table 2 summarizes the key device parameters measured for pristine PBTTT, Si-PBTTT FETs, and Si (with oxide shell)-PBTTT devices. This suggests that the desired enhanced conductivity path of PBTTT-Si NW-PBTTT is prevented by the oxide shell. Hence, a removal of the oxide coating is essential to the processing of these hybrid devices.

Figure 7 shows device performance data measured periodically over 600 h after fabrication. Our hybrid transistors were relatively stable in ambient conditions (exposed to air, moisture, and indoor light) with a reduction of 20% in mobility (from 0.101 to $0.080 \text{ cm}^2 \text{ V}^{-1} \text{ s}^{-1}$) and an ON/OFF ratio remaining higher than 10^5 , demonstrating superior electrical performance without any encapsulation. In contrast, the PBTTT-only devices showed a pronounced degradation with mobility decreased by $\sim 50\%$, and the ON/OFF ratio reduced to 10^3 . Although the interactions and electronic

Table 2. Field Effect Mobility (μ_{FE}), ON/OFF Current Ratio, ON Current (I_{ON}), OFF Current (I_{OFF}), Threshold Voltage (V_T), and Subthreshold Slope (S) of Pristine PBTTT, Si (HF Dipped)-PBTTT, and Si (with SiO_2 Shell)-PBTTT FET Devices at $V_{DS} = -50$ V

FET	HF dip (10 s)	μ_{FE} ($\text{cm}^2 \text{ V}^{-1} \text{ s}^{-1}$)	ON/OFF current ratio	I_{ON} (A)	I_{OFF} (A)	V_T (V)	S (V decade $^{-1}$)
PBTTT	yes	0.031	4×10^4	-2×10^{-4}	-5×10^{-9}	-13	2.551
Si-PBTTT (no SiO_2 shell)	yes	0.101	1×10^7	-1×10^{-3}	-1×10^{-10}	-11	0.258
Si-PBTTT* (with SiO_2 shell)	no	0.035	1×10^5	-2×10^{-4}	-2×10^{-9}	-11	2.175

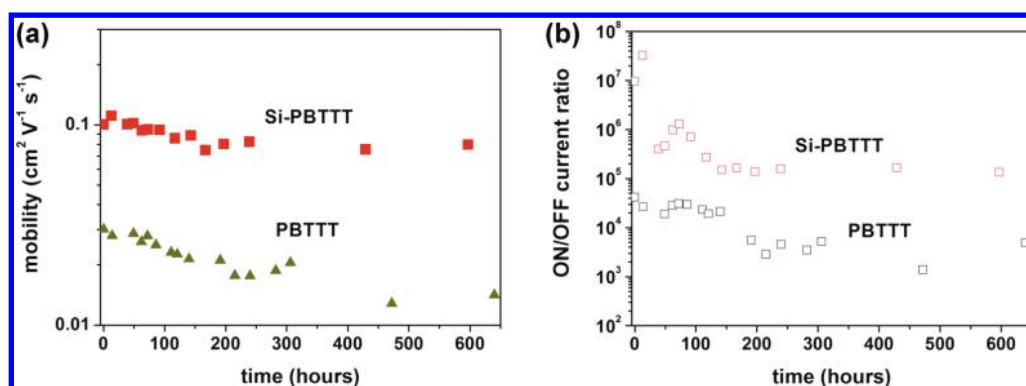


Figure 7. Transistor performance parameters versus time plots for a hybrid Si-PBTTT FET and a organic pristine PBTTT FET. (a) Change in saturation mobility and (b) change in ON/OFF current ratio with time. The devices were stored and performed at room temperature under ambient conditions of air, moisture (50–60% in relative humidity), and indoor light.

properties at the interface between the polymer chains and the NWs are not fully understood yet, our results highlight that this heterogeneous interface plays an important role in the mobility degradation, i.e., improving resistance to oxygen doping.

For hybrid inorganic–organic FET applications, there is plenty of room for further enhancement via a variety of NWs with p-channel, n-channel, or ambipolar semiconductor properties. Further experiments will examine the effect of different network densities and orientations of NWs on the hybrid FET characteristics. Ambipolar NWs would be of most interest for the realization of CMOS devices such as inverters or oscillators.

CONCLUSIONS

In summary, stretched contact printing provides a simple, convenient, and low-cost method to fabricate highly oriented 1-D nanostructure networks over large areas. It is easily applicable to a variety of substrates and materials, including inorganic NWs, CNTs, and organic NWs and uniquely compatible to both solution-based dispersions and as-grown nanostructures supported on substrates. The various fabricated device structures, ranging from single- and multi-NW FETs to hybrid NW-polymer FETs, demonstrate the potency and feasibility of this technique for different electronic applications.

AUTHOR INFORMATION

Corresponding Author

*E-mail cwh31@nctu.edu.tw, Tel +886 (0) 6303 2121 ext 57797, Fax +886 (0) 6303 2535 (G.-W.H.). E-mail wim@eng.cam.ac.uk, Tel +44 (0) 1223 748333, Fax +44 (0) 1223 748348 (W.I.M.).

Notes

The authors declare no competing financial interest.

ACKNOWLEDGMENTS

We thank Merck for the organic semiconductors. G.-W.H. acknowledges support from the W. Wing Yip & Brothers Bursary Award.

REFERENCES

- (1) Sirringhaus, H.; Kawase, T.; Friend, R. H.; Shimoda, T.; Inbasekaran, M.; Wu, W.; Woo, E. P. *Science* **2000**, *290*, 2123–2126.
- (2) Forrest, S. R. *Nature* **2004**, *428*, 911–918.
- (3) Dimitrakopoulos, C. D.; Malenfant, P. R. L. *Adv. Mater.* **2002**, *14*, 99–117.
- (4) Reese, C.; Roberts, M.; Ling, M.-M.; Bao, Z. *Mater. Today* **2004**, *7*, 20–27.
- (5) Salleo, A. *Mater. Today* **2007**, *10*, 38–45.
- (6) Bo, Z. Y.; Lee, C. Y.; Strano, M. S.; Goldfinger, M.; Nuckolls, C.; Blanchet, G. B. *Appl. Phys. Lett.* **2005**, *86*, 182102.
- (7) Xu, Z.-X.; Roy, V. A. L.; Stallinga, P.; Muccini, M.; Toffanin, S.; Xiang, H.-F.; Che, C.-M. *Appl. Phys. Lett.* **2007**, *90*, 223509.
- (8) Liu, S.; Mannsfeld, S. C. B.; LeMieux, M. C.; Lee, H. W.; Bao, Z. *Appl. Phys. Lett.* **2008**, *92*, 053306.
- (9) Park, Y. D.; Lim, J. A.; Jang, Y.; Hwang, M.; Lee, H. S.; Lee, D. H.; Lee, H.-J.; Baek, J.-B.; Cho, K. *Org. Electron.* **2008**, *9*, 317–322.
- (10) Li, F. M.; Hsieh, G.-W.; Dalal, S.; Newton, M.; Stott, J. E.; Hiralal, P.; Nathan, A.; Warburton, P. A.; Unalan, H. E.; Beecher, P.; Robinson, I.; Flewitt, A. J.; Amaratunga, G.; Milne, W. I. *IEEE Trans. Electron Devices* **2008**, *55*, 3001–3011.
- (11) Dietmueller, R.; Stegner, A. R.; Lechner, R.; Niesar, S.; Pereira, R. N.; Brandt, M. S.; Ebbers, A.; Trocha, M.; Wiggers, H.; Stutzmann, M. *Appl. Phys. Lett.* **2009**, *94*, 113301.
- (12) Hsieh, G.-W.; Li, F. M.; Beecher, P.; Nathan, A.; Wu, Y.; Ong, B. S.; Milne, W. I. *J. Appl. Phys.* **2009**, *106*, 123706.
- (13) Huang, Y.; Duan, X.; Wei, Q.; Lieber, C. M. *Science* **2001**, *291*, 630–633.
- (14) Duan, X.; Niu, C.; Sahi, V.; Chen, J.; Parce, J. W.; Empedocles, S.; Goldman, J. L. *Nature* **2003**, *425*, 274–278.
- (15) Park, J. U.; Meitl, M. A.; Hur, S. H.; Usrey, M. L.; Strano, M. S.; Kenis, P. J. A.; Rogers, J. A. *Angew. Chem., Int. Ed.* **2006**, *45*, 581–585.
- (16) Kim, P.; Baik, S.; Suh, K. *Small* **2008**, *4*, 92–95.
- (17) Diehl, M. R.; Yaliraki, S. N.; Beckman, R. A.; Barahona, M.; Heath, J. R. *Angew. Chem., Int. Ed.* **2002**, *41*, 353–356.
- (18) Hu, Z.; Fischbein, M. D.; Querner, C.; Drndić, M. *Nano Lett.* **2006**, *6*, 2585–2591.
- (19) Lee, M.; Im, J.; Lee, B. Y.; Myung, S.; Kang, J.; Huang, L.; Kwon, Y. K.; Hong, S. *Nat. Nanotechnol.* **2006**, *1*, 66–71.
- (20) Hangarter, C. M.; Rheem, Y.; Yoo, B.; Yang, E.-H.; Myung, N. V. *Nanotechnology* **2007**, *18*, 205305.
- (21) Fan, D. L.; Cammarata, R. C.; Chien, C. L. *Appl. Phys. Lett.* **2008**, *92*, 093115.
- (22) Li, M.; Bhiladvala, R. B.; Morrow, T. J.; Siooss, J. A.; Lew, K.-K.; Redwing, J. M.; Keating, C. D.; Mayer, T. S. *Nat. Nanotechnol.* **2008**, *3*, 88–92.
- (23) Kim, F.; Kwan, S.; Akana, J.; Yang, P. *J. Am. Chem. Soc.* **2001**, *123*, 4360–4361.
- (24) Jin, S.; Whang, D.; McAlpine, M. C.; Friedman, R. S.; Wu, Y.; Lieber, C. M. *Nano Lett.* **2004**, *4*, 915–919.
- (25) Jia, L.; Zhang, Y.; Li, J.; You, C.; Xie, E. *J. Appl. Phys.* **2008**, *104*, 074318.
- (26) Yu, G.; Cao, A.; Lieber, C. M. *Nat. Nanotechnol.* **2007**, *2*, 372–377.
- (27) Yu, G.; Li, X.; Lieber, C. M.; Cao, A. *J. Mater. Chem.* **2008**, *18*, 728–734.
- (28) Sharma, R.; Strano, M. S. *Adv. Mater.* **2009**, *21*, 60–65.

- (29) Javey, A.; Nam, S.; Friedman, R. S.; Yan, H.; Lieber, C. M. *Nano Lett.* **2007**, *7*, 773–777.
- (30) Fan, Z.; Ho, J. C.; Jacobson, Z. A.; Yerushalmi, R.; Alley, R. L.; Razavi, H.; Javey, A. *Nano Lett.* **2008**, *8*, 20–25.
- (31) Im, J.; Lee, I.-H.; Lee, B. Y.; Kim, B.; Park, J.; Yu, W.; Kim, U. J.; Lee, Y. H.; Seong, M.-J.; Lee, E. H.; Min, Y.-S.; Hong, S. *Appl. Phys. Lett.* **2009**, *94*, 053109.
- (32) Hsieh, G. W.; Beecher, P.; Li, F. M.; Servati, P.; Colli, A.; Fasoli, A.; Chu, D.; Nathan, A.; Ong, B.; Robertson, J.; Ferrari, A. C.; Milne, W. I. *Physica E* **2008**, *40*, 2406–2413.
- (33) Chang, Y.-K.; Hong, F. C.-N. *Nanotechnology* **2009**, *20*, 195302.
- (34) Fan, Z.; Ho, J. C.; Takahashi, T.; Yerushalmi, R.; Takei, K.; Ford, A. C.; Chueh, Y. L.; Javey, A. *Adv. Mater.* **2009**, *21*, 3730–3743.
- (35) Pevzner, A.; Engel, Y.; Elnathan, R.; Ducobni, T.; Ben-Ishai, M.; Reddy, K.; Shpaisman, N.; Tsukernik, A.; Oksman, M.; Patolsky, F. *Nano Lett.* **2010**, *10*, 1202–1208.
- (36) Hur, S.-H.; Kocabas, C.; Gaur, A.; Park, O. O.; Shim, M.; Rogers, J. A. *J. Appl. Phys.* **2005**, *98*, 114302.
- (37) Kang, S. J.; Kocabas, C.; Kim, H.-S.; Cao, Q.; Meitl, M. A.; Khang, D.-Y.; Rogers, J. A. *Nano Lett.* **2007**, *7*, 3343–3348.
- (38) McAlpine, M. C.; Ahmad, H.; Wang, D.; Heath, J. R. *Nat. Mater.* **2007**, *6*, 379–384.
- (39) Jiao, L.; Fan, B.; Xian, X.; Wu, Z.; Zhang, J.; Liu, Z. *J. Am. Chem. Soc.* **2008**, *130*, 12612–12613.
- (40) Ishikawa, F. N.; Chang, H.-K.; Ryu, K.; Chen, P.-C.; Badmaev, A.; Gomez De Arco, L.; Shen, G.; Zhou, C. *ACS Nano* **2008**, *3*, 73–79.
- (41) Shulaker, M. M.; Wei, H.; Patil, N.; Provine, J.; Chen, Y.-H.; Wong, H.-S. P.; Mitra, S. *Nano Lett.* **2011**, *11*, 1881–1886.
- (42) Xu, F.; Durham, J. W.; Wiley, B. J.; Zhu, Y. *ACS Nano* **2011**, *5*, 1556–1563.
- (43) Hofmann, S.; Sharma, R.; Wirth, C. T.; Cervantes-Sodi, F.; Ducati, C.; Kasama, T.; Dunin-Borkowski, R. E.; Drucker, J.; Bennett, P.; Robertson, J. *Nat. Mater.* **2008**, *7*, 372–375.
- (44) Briseno, A. L.; Mannsfeld, S. C. B.; Reese, C.; Hancock, J. M.; Xiong, Y.; Jenekhe, S. A.; Bao, Z.; Xia, Y. *Nano Lett.* **2007**, *7*, 2847–2853.
- (45) Ogata, K.; Sutter, E.; Zhu, X.; Hofmann, S. *Nanotechnology* **2011**, *22*, 365305.
- (46) Colli, A.; Fasoli, A.; Beecher, P.; Servati, P.; Pisana, S.; Fu, Y.; Flewitt, A. J.; Milne, W. I.; Robertson, J.; Ducati, C.; De Franceschi, S.; Hofmann, S.; Ferrari, A. C. *J. Appl. Phys.* **2007**, *102*, 034302.
- (47) Weber, W. M.; Geelhaar, L.; Graham, A. P.; Unger, E.; Duesberg, G. S.; Liebau, M.; Pamler, W.; Chèze, C.; Riechert, H.; Lugli, P.; Kreupl, F. *Nano Lett.* **2006**, *6*, 2660–2666.
- (48) Cai, Q. J.; Chan-Park, M. B.; Zhang, J.; Gan, Y.; Li, C. M.; Chen, T. P.; Ong, B. S. *Org. Electron.* **2008**, *9*, 14–20.
- (49) McCulloch, I.; Heeney, M.; Bailey, C.; Genevicius, K.; MacDonald, I.; Shkunov, M.; Sparrowe, D.; Tierney, S.; Wagner, R.; Zhang, W.; Chabinyc, M. L.; Kline, R. J.; McGehee, M. D.; Toney, M. F. *Nat. Mater.* **2006**, *5*, 328–333.